Stability Boundaries for Aircraft with Unstable Lateral-Directional Dynamics and Control Saturation

Prakash C. Shrivastava* and Robert F. Stengel†
Princeton University, Princeton, New Jersey

Aircraft that do not possess inherent (aerodynamic) stability must rely on closed-loop control systems for stable operation. Because there are limits on the deflections of an aircraft's control surfaces, the region of stable operation also is bounded. These boundaries are investigated for a lateral-directional example in which vertical fin size is inadequate to provide directional stability and where aileron and rudder deflections are subject to saturation. Fourth-order models are used in this study, with flight control logic based on minimum-control-energy linear-quadratic-regulatory theory. It is found that the stability boundaries can be described by *unstable* limit cycles surrounding stable equilibrium points. Variations in regions of stability with gain levels and command inputs are illustrated. Current results suggest guidelines for permissible limits on the open-loop instability of an aircraft's lateral-directional modes.

Introduction

THE performance and flying qualities of future aircraft will be greatly affected by advanced flight control systems, which can augment stability and command response over the entire flight envelope. Aerodynamic stability need not be built into an aircraft if control effectiveness and power are sufficient to maintain stability by feedback. Unstable aircraft depend on their flight control systems to achieve stability, but constraints on the magnitudes of control deflections limit the region of stable operation. The size and shape of the region of stability depend on the degree of instability, the maximum control forces and moments available, and the feedback control logic.

In Ref. 1, an analysis and design of a stability augmentation system (SAS) for an aircraft with longitudinal static instability and elevator saturation are presented. Analysis of control saturation in command response of statically unstable aircraft is presented in Ref. 2. In these investigations, the stability and saturation boundaries were found to be parallel if a minimum-control-energy (MCE) linear-quadratic (LQ) control law was used. However, the investigation was limited to the case of a single saturating control with a saddle-point phase-plane singularity. The stability boundaries for single-input systems with other types of singularities, e.g., unstable nodes and unstable foci, are presented in Refs. 3 and 4. These analyses were performed using normal-mode coordinates, which simplified determination of the stability boundaries. The stability boundaries were shown to depend on the type of singularities and the magnitude of the feedback gains. For unstable nodes and foci, the stability boundaries were shown to be unstable limit cycles.

This paper examines the effects of control saturation on unstable lateral-directional dynamics. Linear dynamic models of lateral-directional motion are reviewed. Stability boundaries are compared for two cases of directional instability. Since high-gain controllers often are used to increase the system performance, effects of high gains on the regions of stability are examined. The control saturation analysis is extended to determine the changes in stability boundaries with commands.

Presented as Paper 85-1948 at the AIAA Guidance , Navigation, and Control Conference, Snowmass, CO, Aug. 19-21, 1985; received Sept. 9, 1985; revision received Oct. 9, 1987.

*Doctoral Candidate, Department of Mechanical and Aerospace Engineering; currently, Member of the Advanced Engineering Staff, General Motors Corporation.

†Professor, Department of Mechanical and Aerospace Engineering. Associate Fellow AIAA.

Fundamental Analysis of Control Saturation

Control displacement saturation effects are considered using a linear perturbation model of the form

$$\dot{x} = Fx + Gu \tag{1}$$

The state vector x contains the yaw rate r, sideslip angle β, roll rate p, and roll angle ϕ; the control vector u contains rudder and aileron positions δr, δa. The matrices F and G contain dimensional stability derivatives[5] as defined below. In the examples considered here, F has eigenvalues with positive real parts, i.e., the system is open-loop unstable, and the control variable u is constrained to lie within the limits $\pm u_m$.

$$F = \begin{bmatrix} N_r & N_\beta & N_p & 0 \\ -1 & Y_\beta/V_0 & 0 & g/V_0 \\ L_r & L_\beta & L_p & 0 \\ 0 & 1 & 0 & 0 \end{bmatrix} \tag{2}$$

$$G = \begin{bmatrix} N_{\delta r} & N_{\delta a} \\ 0 & 0 \\ L_{\delta r} & L_{\delta a} \\ 0 & 0 \end{bmatrix} \tag{3}$$

Closed-Loop Control Effects

LQ control theory is used to specify a stability augmentation system.[6] The control law obtained is of the form

$$u = -Cx = \begin{bmatrix} \delta_r \\ \delta_a \end{bmatrix} = \begin{bmatrix} c_{11} & c_{12} & c_{13} & c_{14} \\ c_{21} & c_{22} & c_{23} & c_{24} \end{bmatrix} \begin{bmatrix} r \\ \beta \\ p \\ \phi \end{bmatrix} \tag{4}$$

This LQ closed-loop regulator is guaranteed to remain stable as long as all the controls remain unsaturated; however, no such guarantee can be made if one or both of the controls are subject to saturation. With no command inputs, trajectories beginning at certain locations in the state space will converge to the origin, which is a stable equilibrium point of the unsaturated system, whereas other trajectories will diverge. Stability regions can include regions of saturated control, whereas regions of instability can include regions of unsaturated control.

The boundaries between saturated and unsaturated regions are found directly from Eq. (4). Each fixed (saturated) level of scalar control defines a hyperplane separating saturated and unsaturated regions in the state space; hence, there are nine distinctly different regions corresponding to no-satuation or to positive- or negative-saturation of one or both controls in this two-control example. Within these regions, there are up to nine different equilibrium points and four sets of eigenvalues and eigenvectors. For zero command input, asymptotic stability is defined as the tendency for trajectories to approach the single equilibrium point at the origin; therefore, stable trajectories may pass through regions with positive eigenvalues, and unstable trajectories may transit regions with negative eigenvalues. Whether or not a trajectory is convergent depends on the location of equilibrium points, as well as the signs of the eigenvalues. The same is true for nonzero command inputs, except that the stable equilibrium point is no longer at the origin.

MCE Control Law

The LQ control law approaches the MCE solution (in the limit) as the diagonal elements of the control weighting matrix approach infinity. High control weighting leads to low feedback gains and so saturation tends to occur at high levels of feedback state magnitude. Because the cost on control usage is very high, the stable poles are not shifted by the feedback control, but the unstable poles are reflected to their stable left-half s-plane images.[6]

Normal-Mode Coordinates

Analysis of control saturation effects is facilitated by transforming the original state vector into the normal-mode coordinates of the open-loop system. The transformation to the normal-mode coordinate system is obtained by

$$x = Mq \tag{5}$$

where M is the modal matrix and q the normal-mode vector associated with the diagonal system $M^{-1}x$. The corresponding dynamic equation is

$$\dot{q} = \Lambda q + \Xi u \tag{6}$$

where Λ is a diagonal matrix of eigenvalues $\text{diag}(\lambda_1, \lambda_2, \ldots \lambda_n)$, and $\Xi = M^{-1}G$.

This mathematical model can be written as

$$\begin{bmatrix} \dot{q}_u \\ \dot{q}_s \end{bmatrix} = \begin{bmatrix} F_u & 0 \\ 0 & F_s \end{bmatrix} \begin{bmatrix} q_u \\ q_s \end{bmatrix} + \begin{bmatrix} G_u \\ G_s \end{bmatrix} u \tag{7}$$

where q_u and q_s represent unstable and stable modal states, the matrices F_u and F_s the unstable and stable dynamics, and G_u and G_s the corresponding control matrix components.

The MCE control law in the normal-mode space is of the form

$$u = [-C_u \; 0] \begin{bmatrix} q_u \\ q_s \end{bmatrix} \tag{8}$$

Substitution of this control law into Eq. (7) yields the lower-block-triangular closed-loop system

$$\begin{bmatrix} \dot{q}_u \\ \dot{q}_s \end{bmatrix} = \begin{bmatrix} F_u - G_u C_u & 0 \\ -G_s G_u & F_s \end{bmatrix} \begin{bmatrix} q_u \\ q_s \end{bmatrix} \tag{9}$$

which can also be written as

$$\dot{q}_u = (F_u - G_u C_u) q_u \tag{10}$$

$$\dot{q}_s = F_s q_s - G_s C_u q_u \tag{11}$$

Eigenvectors associated with all the modes are changed. The equations of the unstable modes remain uninfluenced by the stable modes, but the stable mode equation has a driving term that consists of the states of the unstable mode and the feedback gain. In the steady state, the origin represents the stable equilibrium point for this system. Since there is no contribution from the stable modes to the trajectories of the unstable modes, the saturation and stability boundaries of the entire system are confined to the plane of unstable mode coordinates. Taken two components at a time, projections of trajectories and intersections of saturation/stability boundaries can be plotted in conventional phase-plane fashion. Single-unstable-root cases lead to open stability boundaries, whereas a pair of real or complex unstable roots causes closed boundaries. Once the boundaries are determined in the normal-mode space, they can be transformed back to the original state space using the inverse transformation.

Determination of Phase-Plane Stability Boundaries

Consider the normal-mode equations with positive saturated control $+u_m$, given by

$$\dot{q}_1(t) = \lambda_1 q_1(t) + b_1 u_m \tag{12}$$

$$\dot{q}_2(t) = \lambda_2 q_2(t) + b_2 u_m \tag{13}$$

The above system has a saddle-point singularity when only one of the eigenvalues is positive, and it has an unstable node singularity when both the eigenvalues are positive. The equilibrium values can be obtained by setting the derivatives $\dot{q}_1$ and $\dot{q}_2$ to zero. Then, q_1^* and q_2^* are

$$q_1^* = -b_1 u_m / \lambda_1 \tag{14}$$

$$q_2^* = -b_2 u_m / \lambda_2 \tag{15}$$

Because the LQ control law can be written as

$$u(t) = -c_{11} q_1(t) - c_{12} q_2(t) \tag{16}$$

the normal-mode saturation boundaries are given by the above equation, substituting $u = \pm u_m$. Since Eqs. (12) and (13) are decoupled, each can be solved independently, yielding

$$q_1(t) = [q_{10} + (b_1 u_m)/\lambda_1 e^{\lambda_1(t)}] + (b_1 u_m)/(-\lambda_1) \tag{17}$$

$$q_2(t) = [q_{20} + (b_2 u_m)/\lambda_2 e^{\lambda_2(t)}] + (b_2 u_m)/(-\lambda_2) \tag{18}$$

Saddle-Point Case

The saddle-point case is obtained when $\lambda_1 < 0$ and $\lambda_2 > 0$. For those initial conditions that make the signs of the coefficient of the exponent corresponding to the unstable mode λ_2 [Eq. (18)] and the constant term differ, the trajectories converge toward the saturation boundary; the trajectories diverge when these terms have the same sign. The system remains at its equilibrum value for those initial conditions where the coefficient of the exponent in Eq. (18) vanishes. This requirement is met by the axes of the unstable modes passing through the saturated equilibrium points, which are always located in the saturated regions[4]; hence, they represent parts of the stability

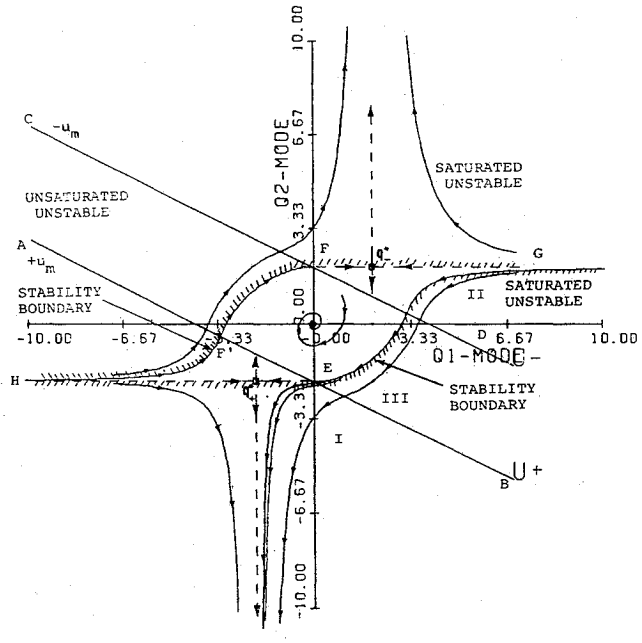

a) Feedback of stable and unstable modes

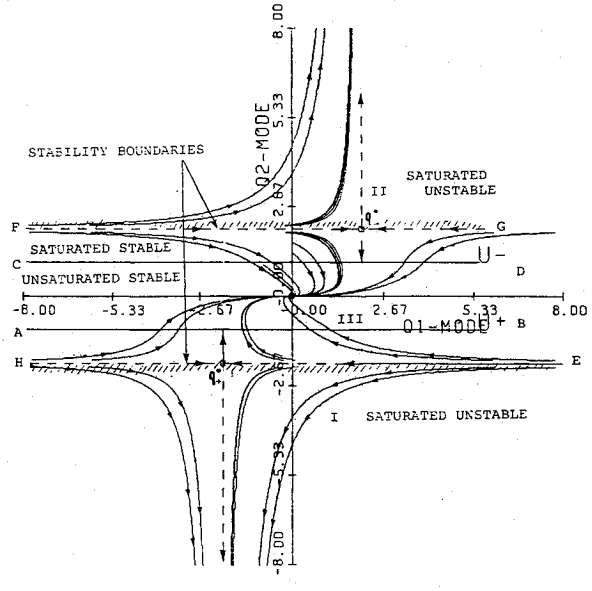

b) Feedback of unstable mode only

Fig. 1 Stability boundaries for saddle-point case (normal-mode coordinates).

boundaries in the saturated regions. When both the modal coordinates are fed back, the saturation boundaries intersect the axes of the normal modes.

The portions of the stability boundaries through the unsaturated regions are determined by the dynamics of the closed-loop system using the points of intersections of the saturation boundaries and the axes of the unstable mode, as illustrated in Fig. 1a. When only the unstable mode is fed back, the saturation boundaries are parallel to the unstable-mode axes emanating from the saturated equilibrium points. These axes represent the complete stability boundaries in the normal-mode coordinates, as shown in Fig. 1b.

Unstable Node Case

The unstable node case is obtained when λ_1 and λ_2 are positive. For this system to be stabilized, both modes must be fed back; hence, the saturation boundaries always would be inclined to the normal-mode axes, and stability boundaries

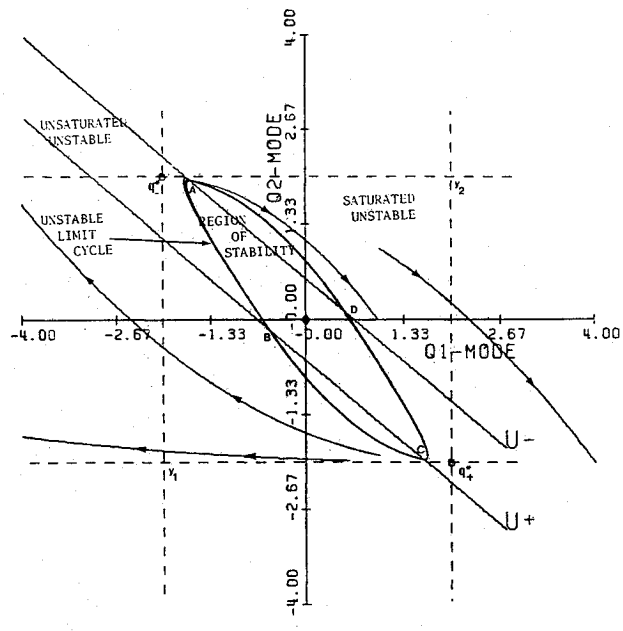

Fig. 2 Stability boundaries for unstable node case (normal-mode coordinates).

similar to Fig. 1b are ruled out. Since the equilibrium points due to control saturation are always located outside the saturated region,[4] boundaries similar to Fig. 1a are not possible. With $\lambda_1 > 0$, the trajectories converge when the signs of each coefficient of the exponents and the constant terms in Eqs. (17) and (18) are opposite. In this case, only parts of the q_1 and q_2 axes within the equilibrium values contain stable regions (Fig. 2).

The rectangle formed by the equilibrium axes establishes the outside limit for the stability region. There is a stable singular point within the linear region at the origin, and neighboring trajectories can be forced to the origin. Therefore, one can anticipate existence of an unstable limit cycle that encloses a stable equilibrium point. Any small perturbation of the motion from this limit cycle would result in a departure to either the unstable region or the origin. A general closed-form analytical expression for this limit cycle cannot be determined; hence, an algebraic test to determine whether an initial condition lies within or outside the limit cycle is difficult to find. However, the unstable limit cycle can be obtained numerically by integrating the system of equations backward in time, with initial conditions in the vicinity of the origin.

Effects of Command Inputs

Command augmentation systems (CAS) are designed to achieve desired equilibrium values and suitable system response to external commands. The CAS commands the state to nonzero equilibrium value, and it may modify transient response by closed-loop control.[7] In this study the desired output is represented by

$$y(t) = H_x x(t) \tag{19}$$

and so state equilibrium implies command equilibrium as well:

$$y^* = H_z x^* \tag{20}$$

Following Ref. 7, the nonsingular command augmentation control law can be written as

$$u(t) = C_F y^* + C_B x(t) \tag{21}$$

with

$$C_F = (-H_x F^{-1} G)^{-1} + C(-F^{-1} G)(-H_x F^{-1} G)^{-1} \tag{22}$$

$$C_B = -C \tag{23}$$

The system's closed-loop response to the command is described by

$$\dot{x}(t) = (F + GC_B)x(t) + GC_F y^* \tag{24}$$

The eigenvalues and eigenvectors of Eq. (24) are associated only with $(F+GC_B)$, and so the choice of the command vector has no effect on these parameters. From Eq. (21) it is clear that the saturation boundaries vary with changes in the command vector; therefore, the stability boundaries also vary. Nonzero command vectors yield saturation boundaries that are asymmetric with respect to the origin. The feedback gain C_B affects only the closed-loop eigenvalues; it has no effect on the value of u^* for a desired command. Control saturation limits $\pm u_m$ determine the system's ability to achieve the command vectors in the steady state. Desired outputs (i.e., constant commands) that cause the control to violate the limits

$$-u_m \leq u^* \leq +u_m$$

cannot be attained. Consequently, the minimum and maximum values of the equilibrium states for the above saturation limits are given by

$$x^*_{\max/\min} = \pm F^{-1} G u_m \tag{25}$$

and the maximum/minimum values of command vectors that can be commanded and achieved are given by

$$y^*_{\max/\min} = H_x x^*_{\max/\min} \tag{26}$$

In state-space coordinates, x^* lies on a hyperplane determined by Eq. (25); therefore, command vectors produce equilibrium states that lie on this hyperplane. At control saturation limits $\pm u_m$, the saturated and unsaturated equilibrium points sought by the command vector coincide, and they lie on the saturation boundary. Variations in the command vector change the location of the desired equilibrium point and saturation boundaries. The locations of equilibrium points with all controls saturated do not change, but the locations of equilibrium points with one of the controls saturated change with the commands. Because of this change in the single-control-saturated equilibrium points relative to fixed all-control-saturated equilibrium points, the shapes and sizes of the stability boundaries change with the command vector.

The maximum and minimum values of attainable state equilibrium depend upon the control saturation limits and the open-loop dynamics, and control saturation limits set bounds on the achievable command vector y^*. Although achievable command vectors are independent of the feedback gain C_B, transient response can impact the region of achievable output vectors. If, for example, the transient response to an "achievable" command momentarily forces the state into a divergent region, then the trajectories can diverge and that commands is not truly achievable.

Effects of Vertical-Fin-Size Reduction on Lateral-Directional Dynamics

In conventional aircraft configurations, the lateral-directional dynamics normally are characterized by the Dutch roll, roll subsidence, and spiral modes; however, reducing the vertical fin size alters the aircraft's response modes.[8,9] With sufficient reduction in fin size, the vertical tail contribution to the static directional stability derivative is reduced, making the nondimensional directional stability derivative C_{n_β} negative. The yaw damping derivative C_{n_r}, control power derivative $C_{n_{\delta_r}}$, and dihedral derivative C_{l_β}, are reduced in magnitude, whereas the roll derivatives and roll-to-yaw coupling derivatives remain relatively unaffected. The effects on dimensional stability derivatives (e.g., N_β) are proportional to the changes in the nondimensional derivatives (e.g., C_{n_β}). The major impact of fin-size reduction is felt on N_β, which becomes negative, making the aircraft directionally unstable. In Ref. 10 it is shown that there always would be two unstable roots.

Numerical Models for Analysis

A high-performance fighter aircraft with stable lateral-directional dynamics was chosen as a baseline model for this study. Nondimensional derivatives for the unstable lateral-directional model were computed for several fin configurations, assuming a sea level, Mach 0.4 flight condition. The dimensional stability derivatives for three fin configurations are presented in Table 1. Case 1 represents the stable baseline model, and cases 2 and 3 represent the unstable models obtained by the fin-size reduction. The numerical values assume that velocity and angles are measured in feet per second and radians, respectively. The rudder and aileron limits are fixed at ± 20 deg for all numerical calculations. The eigenvalues of the open-loop dynamics for the fourth-order models are given in Table 1.

Table 1 Dimensional derivatives eigenvalues for three aircraft configuration

Derivative	Case 1	Case 2	Case 3
$N_{\delta r}$	−0.379	−0.209	−0.177
N_β	3.740	−0.865	−2.029
N_p	−0.104	−0.072	−0.070
Y_β/V_0	−0.258	−0.207	−0.195
L_r	0.736	0.506	0.474
L_β	−11.98	−5.87	−4.98
L_p	−2.51	−2.49	−2.48
$N_{\delta r}$	−6.21	−3.53	−2.96
$N_{\delta a}$	0.287	0.287	0.289
$L_{\delta r}$	5.54	1.96	1.39
$L_{\delta a}$	20.12	20.12	20.12
Eigenvalues	$-0.207+j2.074$	−0.857	−1.396
	$-0.207-j2.074$	0.459	1.143
	−2.72	−2.642	−2.647
	−0.012	0.133	0.0363

Table 2 Minimum-control-energy gains for normal-mode and state coordinates

	Normal-mode coordinates		State-space coordinates			
	q_1	q_2	r	β	p	ϕ
Case 2						
δr	−0.39	−0.15	−0.306	0.246	0.015	0.026
δa	−0.04	0.02	−0.057	0.036	0.005	0.009
Case 3						
δr	−1.33	−0.06	−0.737	0.996	0.032	0.066
δa	−0.24	0.06	−0.141	0.183	0.009	0.019

Effects of Control Saturation on Closed-Loop Lateral-Directional Stability

Linear-quadratic gains in normal-mode coordinates and physical coordinates were computed for the unstable lateral-directional dynamics of case 2 and case 3 configurations. The state weighting matrix was an identity matrix, and the control weightings for the ailerons and rudder were fixed at $R = \text{diag}(500{,}000;500{,}000)$, approximating the MCE case. The MCE gains are given in Table 2. Gains for the rudder controls are higher than gains for aileron control, because the low damping and directional stability caused by small fin size are highly augmented by the rudder control law. Variations in the roll-rate and bank-angle feedback gains to the rudder are small, because the effect of fin-size reduction on the roll mode is small. Eigenvalues for the closed-loop system and saturated rudder or ailerons are given in Table 3.

Figure 3a presents the saturation and stability boundaries in open-loop normal-mode coordinates (q_1,q_2) for case 2. The rudder and aileron saturation boundaries are straight lines, and the stability boundary is a closed curve, an unstable limit cycle. The region enclosed by the limit cycle is the region of stability, and all initial conditions in it converge to the origin. Initial conditions that fall outside this region result in divergence. Note that this limit cycle lies within the saturation boundaries of the aileron; for the given aileron saturation limits, aileron control does not influence the shape or size of the region of stability. For the region of stability to be influenced, either increased aileron feedback gain or reduced aileron saturation control limit is necessary.

Table 3 Eigenvalues with minimum-control-energy gains

	Closed-loop	Rudder saturated	Ailerons saturated
Case 2	−0.459	0.41	0.26
	−0.133	0.07	0.93
	−0.857	−0.85	−1.36
	−2.566	−2.64	−2.64
Case 3	−1.143	1.10	4.56
	−0.0363	−0.11	$-1.2+j0.14$
	−1.396	−1.90	$-1.12-j0.14$
	−2.647	−3.34	−2.64

For the MCE control laws, saturation boundaries in the four-dimensional state space are hyperplanes parallel to the axes of the stable modal coordinates q_3 and q_4. Since the stable modes are unaffected by the MCE control laws, the stability region can be described in the $(q_1$-$q_2)$ plane; hence, it is described by a hypercylinder in the four-dimensional normal-mode space. This hypercyclinder does not intersect the axes of the stable modes, and it transforms to an equivalent hypercylinder in the original state space, as shown below.

The linear transformation given by Eq. (5) can be rewritten as

$$\begin{bmatrix} r \\ \beta \\ p \\ \phi \end{bmatrix} = \begin{bmatrix} T_1 & T_2 \\ T_3 & T_4 \end{bmatrix} \begin{bmatrix} q_1 \\ q_2 \\ q_3 \\ q_4 \end{bmatrix} \tag{27}$$

In Eq. (27), q_1 and q_2 are the points on the limit cycle. Given q_1, q_2, β, and ϕ, the remaining normal-mode coordinates q_3 and q_4 are readily obtained by

$$\begin{bmatrix} q_3 \\ q_4 \end{bmatrix} = T_4^{-1} \left\{ \begin{bmatrix} \beta \\ \phi \end{bmatrix} - T_3 \begin{bmatrix} q_1 \\ q_2 \end{bmatrix} \right\} \tag{28}$$

Substituting Eq. (28) in Eq. (27) then yields the region of stability in the r-p plane, which also is a closed region. The stability boundaries for nonzero sideslip angles are shown in Fig. 3b. Sideslip angle is seen to have a small effect on the stability region, as is true for roll angle (not shown).[10]

Effects of Gain Variations

High-feedback-gain controllers normally are used to reduce the effects of parameter variations, and high-forward-loop gains quicken vehicle response. As a result of high-feedback gain, the closed-loop poles move farther into the left-half s plane; control saturation occurs for relatively small values of state variables, and the region of unsaturated operation is reduced.

To illustrate the effect of high gains on stability boundaries, MCE gains for the case 2 configuration were increased arbitrarily by a factor of five. (The new feedback gains do not

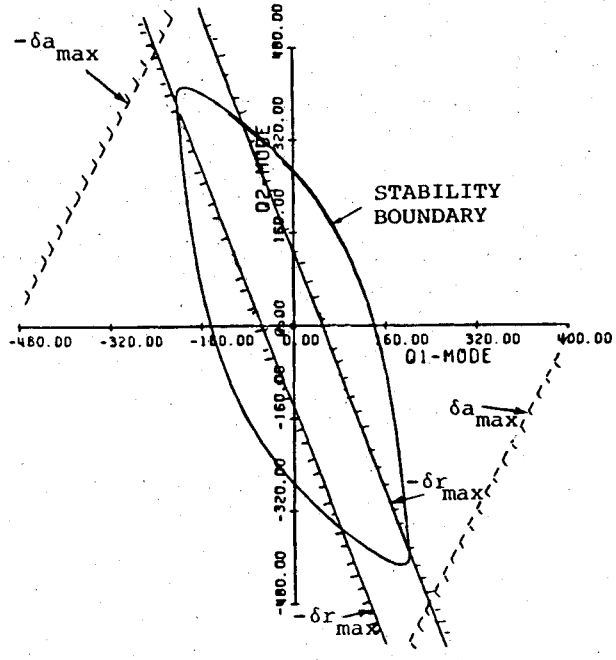

a) Normal-mode coordinates

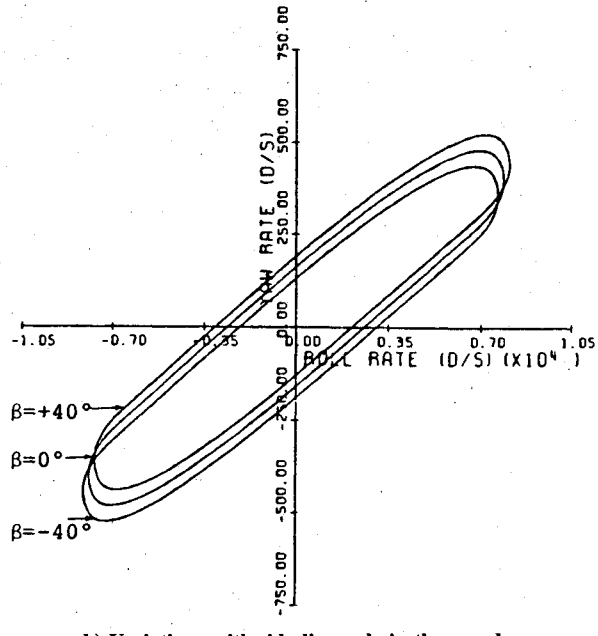

b) Variations with sideslip angle in the r-p plane

Fig. 3 Stability boundaries for case 2 with minimum-control-energy gains.

minimize the original cost function.) Eigenvalues for the closed-loop system and saturated rudder or aileron are given in Table 4. The eigenvalues for MCE and high-gain cases in Tables 3 and 4 show that the high-feedback-gain system is relatively more stable even with saturated rudder or ailerons. Intuitively, the size of the stability region should also increase with increased system stability. The validity of this intuition is illustrated in this example. The saturation and stability boundaries in normal-mode and physical coordinates are shown in Fig. 4. By comparison to Fig. 3a, the size of the stability region is seen to be increased; however, the stability boundary in Fig. 4 passes through the saturated-aileron region, and so the stability region depends on the aileron saturation limits.

Consider the case when elements in the control weighting matrices for the rudder and aileron are not the same. High (low) control weighting on rudder and low (high) control weighting on aileron result in low (high) feedback gains for the rudder and high (low) feedback gains for the aileron, respectively. Although not MCE, high values of control weightings ensure that there is negligible alteration of stable modes. In such cases, the normal-mode stability regions also are hypercylinders parallel to the axes of the stable modes. Thus, the regions of stability in the r-p planes still can be determined using Eqs. (27) and (28).

The effects of low rudder and high aileron weightings (and vice versa) on the stability boundaries are examined, beginning with rudder weighting of 500,000, aileron weighting of 5000, and $Q=I$ (Table 5). Even though the rudder gains are small, saturating the rudder produces a right-half-plane eigenvalue; however, rudder saturation is not likely to be a problem, as shown by the saturation and stability boundaries of Fig. 5. Saturating the ailerons also produces a right-half-plane eigenvalue, indicating that the nominal, two-control system makes use of the yawing moments for both controls. The stability boundaries remain unaffected by the rudder saturation boundary, and the size of this stability region is smaller than that shown in Fig. 3.

The gains and eigenvalues for rudder weighting of 5000 and aileron weighting of 500,000 are given in Table 6, and the

Table 4 Eigenvalues with five times minimum-control-energy gains

	Closed-loop	Rudder saturated	Ailerons saturated
Case 2	−5.164	0.325	0.249
	−0.174	−0.333	−0.882
	−2.642	−0.818	−2.645
	−0.174	−2.682	−8.443
Case 3	−0.221	0.997	0.306
	−1.396	−0.803	−1.493
	−2.646	−2.778	−2.668
	−10.40	−1.283	−6.778

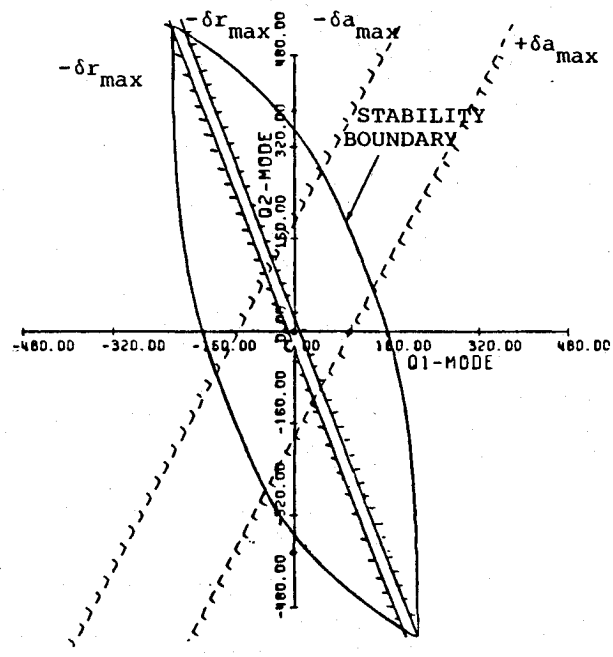

a) Normal-mode coordinates

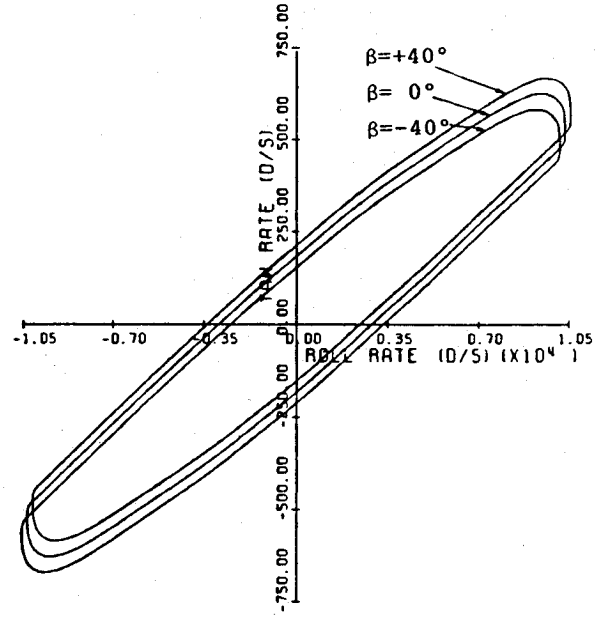

b) Variations with sideslip angle in the r-p plane

Fig. 4 Stability boundaries for case 2 with five times minimum-control-energy gains.

Table 5 Control gains and eigenvalues for case 2 with high rudder weighting

Gains

	Normal-mode coordinates			State vector coordinates		
	q_1	q_2	r	β	p	ϕ
δr	−0.06	−0.02	−0.05	0.039	0.003	0.005
δa	−1.23	−0.26	−1.11	0.836	0.065	0.12

Eigenvalues

Closed-loop	Rudder saturated	Ailerons saturated
−.135	0.30	0.33
−4.6	−2.97	−0.04
−2.64	−1.86	−0.85
−0.86	−0.91	−2.64

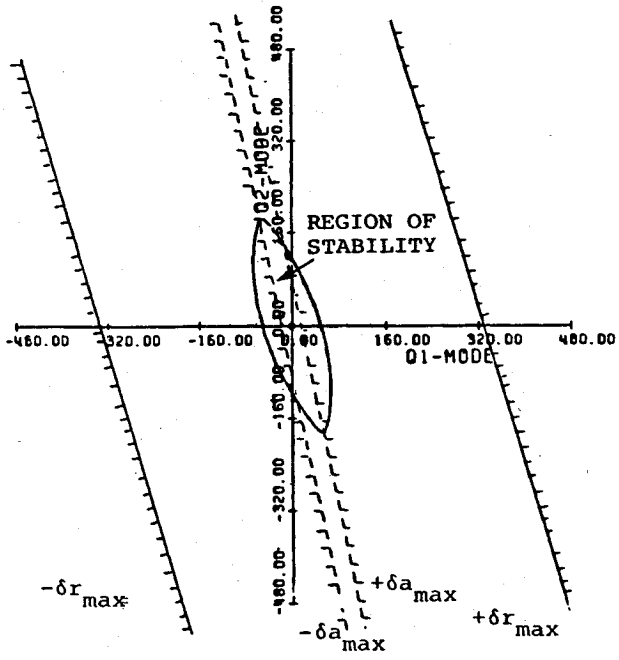

a) Normal-mode coordinates

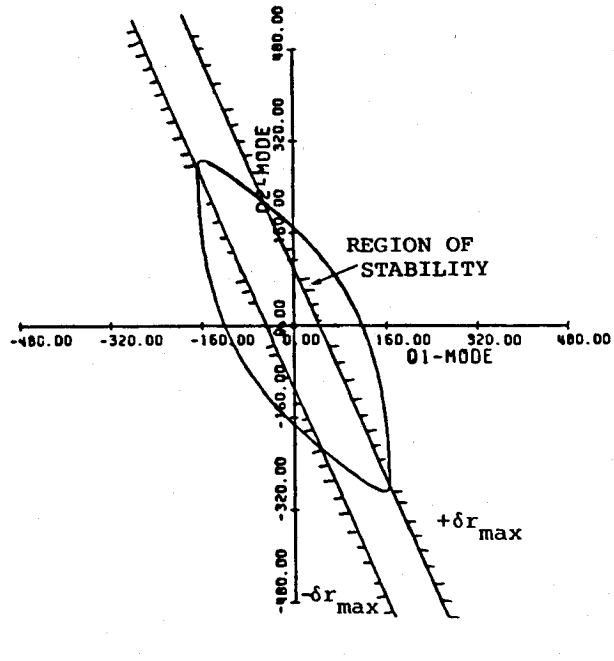

a) $y^* = (0.0, 0.0)$

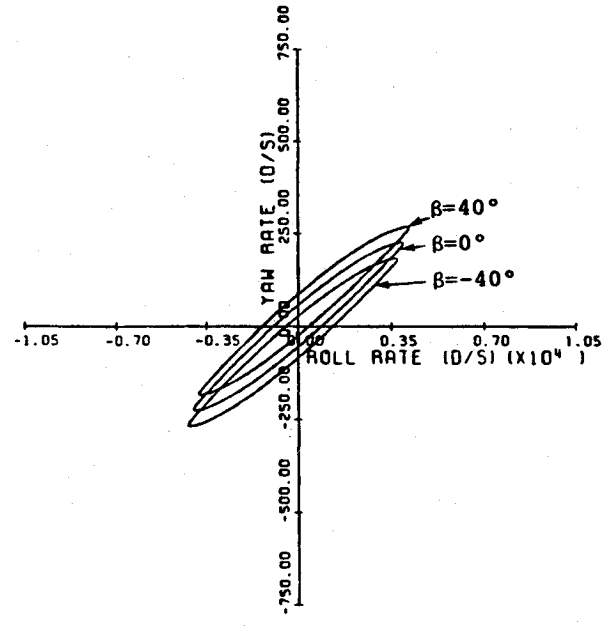

b) Variations with sideslip angle in the *r-p* plane

Fig. 5 Stability boundaries with high rudder weighting for case 2; $R = \text{diag}(500,000;5000)$.

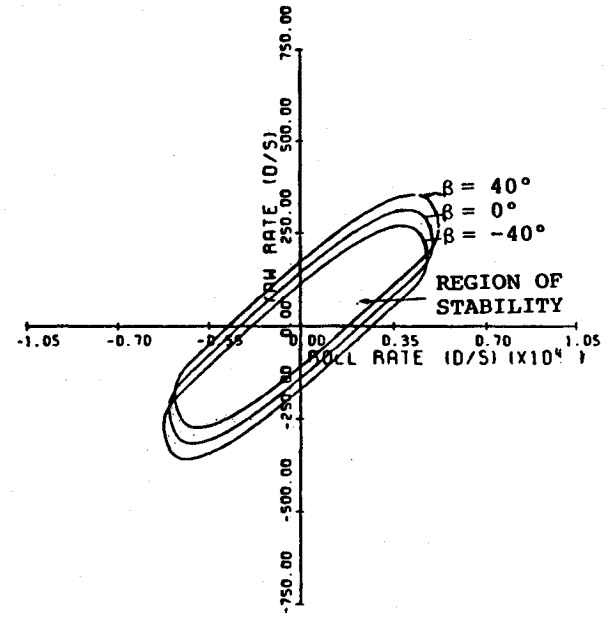

b) Variations with sideslip angle in the *r*-p plane.

Fig. 6 Stability boundaries with high aileron weighting for case 2; $R = \text{diag}(5000;500,000)$.

Table 6 Control gains and eigenvalues for case 2 with high aileron weighting

	Gains					
	Normal-mode coordinates			State vector coordinates		
	q_1	q_2	r	β	p	ϕ
δr	−0.44	−0.19	−0.33	0.27	0.015	0.025
δa	−0.0002	0.0004	−0.0005	0.0003	0.00005	0.00001

Eigenvalues		
Closed-loop	Rudder saturated	Ailerons saturated
−0.14	0.46	0.26
−0.46	0.13	−1.53
−2.64	−2.64	−0.91
−0.86	−0.86	−2.64

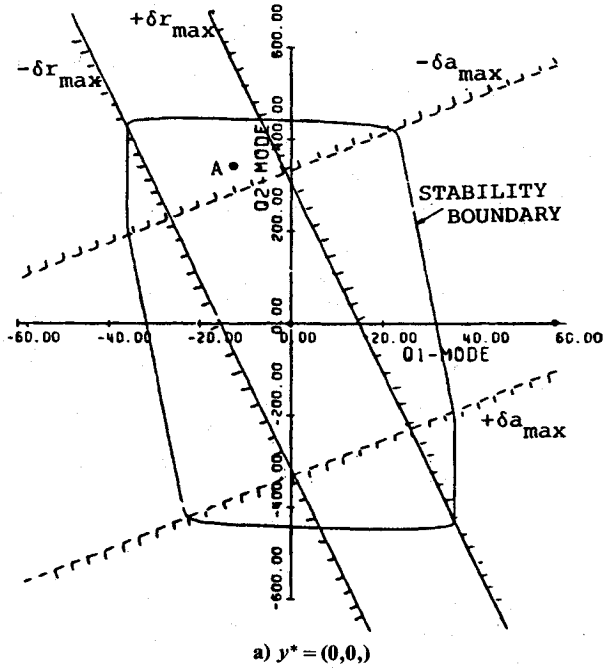

a) $y^* = (0,0,)$

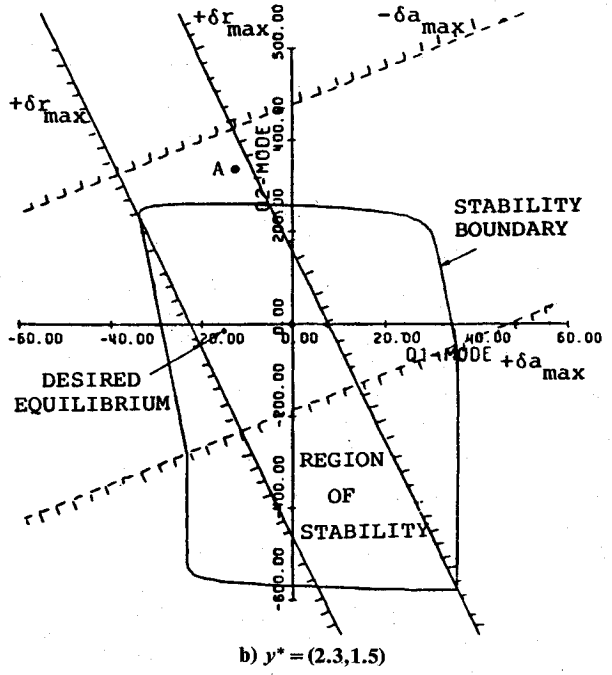

b) $y^* = (2.3,1.5)$

Fig. 7 Variation in stability boundaries with commands; case 3, minimum-control-energy gains (normal-mode coordinates).

saturation and stability boundaries are shown in Fig. 6. The region of stability is larger in size than for the high-rudder-weighting case because high-feedback gains to the rudder provide better directional stability augmentation than feedback to the ailerons, and the stability boundary is invariant with respect to aileron saturation limits. For both cases of unequal control weightings, the variation in the region of stability with sideslip angle is small (Figs. 5b and 6b). Because feedback gains from bank angle to the rudder and ailerons are small, the effect of bank angle on the region of stability is small.

Comparison of the stability boundaries in Figs. 3–7 shows that the largest regions of stability are obtained when the control weightings on the rudder and aileron are equal and that the size of the stability region increases when the feedback gain magnitudes increase. The smallest region of stability is obtained for the high-rudder-weighting case. Nevertheless, although high-feedback gains are desirable for achieving a large stability region, these gains also must satisfy criteria for normal operation in the unsaturated region, which may limit the acceptable gain magnitude. Except for the case of high rudder weighting, the variations in stability regions with sideslip angles are small. Sideslip angle dependency could be ignored if rolling and yawing rates could be restricted to the innermost intersection of all stability regions.

Effects of Command Inputs

Commanded inputs have an effect on system stability because they offset the desired equilibrium point from the origin, and stability boundaries become asymmetrical. The desired equilibrium point may lie close to a stability boundary, and so small disturbances can make the system unstable. This is demonstrated for case 3 using a nonsingular "task-tailored" command vector, in which yaw rate and sideslip angle are commanded independently. (A more conventional command vector would be roll rather than yaw rate; this is a singular-command variable in the sense of Ref. 7.) The output matrix is then $H_x = \text{diag}(1,1)$ and, with the feedback-gain matrix in Table 3, the forward-gain matrix is

$$C_F = \begin{bmatrix} 0.378 & 5.762 \\ 0.278 & 5.412 \end{bmatrix} \tag{29}$$

The desired equilibrium states must lie within the saturation limits which, themselves, shift with the value of the command.

Two sets of command vectors are considered. In the first instance (Fig. 7a) the commands are zero. The saturation boundaries are symmetric about the origin, and the stability boundary generated by backward integration is antisymmetric about the normal axes. Case 3 is more unstable than case 2, and its stability region is, therefore, smaller. Its stability boundary passes through regions in which both rudder and ailerons are saturated.

When the command is changed to $y^* = (2.3,1.5)$, the stability boundary becomes asymmetrical, and no portion of it passes through the region of negative aileron satuation (Fig. 7b). Furthermore, portions of the space that were stable with zero command are no longer stable regions. For example, if a disturbance forces the instantaneous (q_1,q_2) point to be point A as the pilot commands $y^* = (2.3,1.5)$, the system is unstable because point A does not lie within the stable region of that command. It can be concluded that the allowable perturbation space is smaller than the zero-command stability boundary when nonzero commands are issued. Figure 7b also indicates that the allowable command space is smaller than the unsaturated region of the system.

Conclusions

General conditions for stability boundaries of linear systems containing control saturation have been presented. For linear control laws, saturation boundaries always appear as hyperplanes in the normal-mode space. The shape of the stability boundaries depends on the type of open-loop instability. Fourth-order models of lateral-directional aircraft motion exhibit two unstable roots that result from the lack of directional stability. Stability regions for aircraft with directional instability are found to be hypercylinders in the normal-mode space when only unstable modes are fed back; the stable regions can be increased in size by increasing the magnitudes of feedback gain. These boundaries transform to hypercylinders in the original state space. For small directional instabilities, variations in stability regions with sideslip and roll angles are small, and the innermost stability region in the roll rate-yaw rate phase plane can represent the overall region of stability. With increased directional instability, the stability region is reduced, and variations in the regions of stability with sideslip angle become significant. Stability regions are command-dependent, and a possibility of departure exists if

initial conditions at the time of new command initiation lie outside the stability region.

Acknowledgments

This research was sponsored by NASA Langley Research Center, Hampton, Virginia, under Grant NGL 31-001-252.

References

[1]Hanson, G.D. and Stengel, R.F., "Effects of Displacement and Rate Saturation on the Control of Statically Unstable Aircraft," *Journal of Guidance, Control, and Dynamics,* Vol. 7, March–April 1984, pp. 197–205.

[2]Hanson, G.D. and Stengel, R.F., "Effects of Control Saturation on the Command Response of Statically Unstable Aircraft," AIAA Paper 83-0065, Jan. 1983.

[3]Shrivastava, P.C. and Stengel, R.F., "Stability Boundaries for Systems with Control Constraints," *Proceedings of the 18th Annual Conference on Information Sciences and Systems,* Princeton Univ., Princeton, NJ, March 1984.

[4]Shrivastava, P.C. and Stengel, R.F., "Stability Boundaries for Closed-Loop Systems with Control Constraints," *Proceedings of the 23rd IEEE Conference on Decision and Control,* IEEE, New York, Dec. 1984, pp. 1326–1329.

[5]Seckel, E., *Stability and Control of Airplanes and Helicopters,* Academic Press, New York, 1964.

[6]Stengel, R.F., *Stochastic Optimal Control: Theory and Application,* Wiley, New York, 1986.

[7]Stengel, R.F., "Equilibrium Response of Flight Control Systems," *Automatica,* Vol. 18, March 1982, pp. 343–348.

[8]Roskam, J., *Methods for Estimating Stability and Control Derivatives of Conventional Subsonic Airplanes,* Univ. of Kansas, Lawrence, KS, 1973.

[9]Etkin, B., *Dynamics of Flight: Stability and Control,* Wiley, New York, 1959.

[10]Shrivastava, P.C., "Stability Regions of Relaxed Static Stability Aircraft Under Control Constraints," Ph.D. Thesis, Mechanical and Aerospace Engineering Dept., Princeton Univ., Princeton, NJ, Rept. 1747-T,Oct. 1986.